

Application of the spark tracing method to velocity measurements in a sub-millimeter scale gas flow

Mitsuhisa Ichibanagi¹, Yohei Sato² and Koichi Hishida²

¹ Department of Engineering and Applied Sciences, Sophia University, Tokyo, Japan
ichibanagi@sophia.ac.jp

² Department of System Design Engineering, Keio University, Yokohama, Japan

ABSTRACT

A molecular tagging technique using the spark tracing method has been applied to measure velocity distributions in sub-millimeter-scale gas flows that were formed as air jet flows through a sub-millimeter channel. Spark lines were generated by applying a high voltage, based on the air ionization via the electrical discharge phenomena. The velocities using displacements of spark lines were 10–30% smaller than those using the theoretical equation in a rectangular channel. In order to identify the cause of measurement errors, the relationship between the ionized air regions and the gas flow velocities was investigated by the numerical simulation. The simulation reveals that an actual spark line goes through a pathway with a minimum electric resistance, and the velocities from the theoretical equation are agreed with the velocities when the spark line width is assumed to be zero. The results suggest us to propose the new velocity correction technique using the relationship between the spark line widths and the measure velocities. The velocities from the experiments with the correction were agreed well with those from the theoretical equation. Furthermore, the spark tracing method with the correction technique was applied to a mixing air flow through two channels, for the examination of the effect of the gas temperature on the velocity detection.

1. INTRODUCTION

Microfluidic devices have been widely used for biological and chemical analysis applications, e.g., lab-on-a-chip and micro total analysis systems (micro-TAS) [1], [2]. The recent development of microfluidic devices has yielded to analyze not only liquid flows but also gas flows or two-phase flows [3]. The precise control of a small gas volume and molecules in microchannel flows is expected to improve the efficiency of analysis and detection in micro-TAS, which is dependent on the development of accurate measuring techniques. The optical methodology to understand the fluid motion in microchannels is classified into two categories [4]: tracking fluorescent particles and tracing fluorescent dye. Micron-resolution particle image velocimetry (micro-PIV) [5] has become a powerful tool to optimally design the microchannel geometry in the microfluidic devices. Lindken *et al.* [6] and Werely and Meinhart [7] reviewed the recent advances in micro-PIV and the applications to various fields. For improving the spatial resolution, Sadr *et al.* [8] and Kihm *et al.* [9] developed nano-PIV utilizing the evanescent wave that is generated from a total internal reflection of light, and Pouya *et al.* [10] and Freudenthal *et al.* [11] used the quantum dot nanoparticles as the tracer particles. These above-mentioned techniques are, however, limited to the velocity measurements of liquid flows, and there are a few studies of the micro-PIV measurements in gas flows. Kim *et al.* [12] measured the velocity distributions of oscillatory airflows in a bronchiole model by using the oil mists. In the experiments, it was difficult to obtain the accurate velocity distributions, because the density of oil mists is very larger than that of air, and consequently, the oil mists cannot follow up the airflows.

Molecular tagging velocimetry (MTV), that is the technique to tag and trace molecules in the regions of interest, is an alternative optical approach to investigate flow structures. Caged fluorescent dye has been commonly used, because of its high signal-to-noise ratio and its fidelity to the fluid motion. MTV using this dye has been applied to the various flow scale range from the macroscale flows [13], [14] to the microscale flows [15]–[18]. However, this technique is also restricted to the velocity measurements of liquid flows, because this dye is required to dissolve in an aqueous solution. Experimental efforts by Andre *et al.* [19] and Hecht *et al.* [20] measured the velocity distributions in gas flows by using nitrogen monoxide (NO). This technique is based upon the use of gas molecules with the fluorescent properties, and the velocities are evaluated from the displacements of fluorescent tagged regions. The shortcomings of this technique are that there are remarkably few gas molecules with the fluorescence and most of them have the toxic properties, which is not appropriate for the practical use. The spark tracing method is one of the velocity measuring techniques of any gas flows, which has been developed and improved by Nakayama and Aoki [21]. This method is based on the visualization of spark lines, and the velocities of gas flows are calculated from the displacements of their

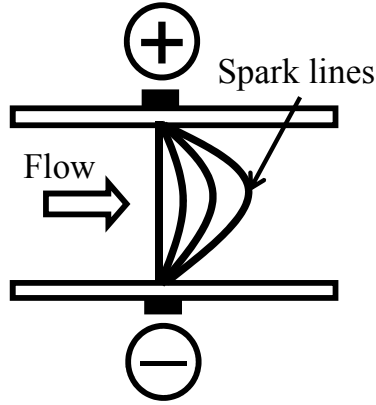


Figure 1: Schematic concept of the spark tracing method using a high voltage system with high frequency.

lines. The lines are generated by applying a high voltage with a high frequency and producing the air ionization via the electrical discharge phenomena. The previous studies have reported the development of high voltage supply [22], the effect of the electrode configuration and applied voltage on the formation of spark lines [22], and the application to various internal flows [23] and external flows [24], [25]. It should be noted from their studies that this method has been able to visualize gas flows and obtain velocity distributions easily and safely, even if the density differences between ionized and unionized air might induce any measurement errors [26].

The objective of the present study is to develop the velocity measuring technique for sub-millimeter-scale gas flows by using the spark tracing method. For the generation of spark lines, we make the high voltage system of a few kV with the high frequency of 1×10^4 Hz by ourselves and prepare several stainless-steel electrodes with a 0.8 mm diameter. The measurement system is based on the high speed CMOS camera of 1×10^4 frames/s equipped with the objective lens, which results in the time resolution of 0.1 ms. In the experiments, single air jet flows with a sub-millimeter-scale are formed through a 0.8 mm-square channel, and their exit velocities are measured whose Reynolds numbers are 65 and 135. Furthermore, for improving the above measurement errors due to the density differences [26], the present study proposes the new velocity correction technique whose availability and validity are confirmed by using the numerical simulation. In addition, the effect of the gas temperature on the velocity detection is discussed by measuring a mixing air jet flow field with different temperatures through two channels.

2. PRINCIPLE OF SPARK TRACING METHOD

2.1 Measurement Principle

Figure 1 illustrates the schematic of the measurement principle of the spark tracing method, which is based on the electrical discharge phenomena. For the generation of spark lines, it is required to set up two electrodes perpendicular to gas flow regions of interest and apply a high voltage with a high frequency. The first voltage application makes the ionized air that is a pathway through spark lines, and the ionized air is maintained at a steady state for approximately 1.0 ms and has an advantage of the superior electrical conductivity, compared with the unionized air. The frequency of second and subsequent applications is set at more than 1×10^3 Hz, and consequently, spark lines go through the pathway of ionized air region. Finally, gas flows are visualized by capturing the spark lines using the high speed CMOS camera.

2.2 Algorithm for Velocity Detection

Figure 2 shows the schematic of the algorithm for the velocity detection using the spark tracing method. The instantaneous image of a spark line in an air jet flow through a channel was captured from the upper side of channel at $t = t_0$ as shown in figure 2 (a), and figure 2 (b) was at $t = t_0 + \Delta t$. Figure 2 (c) exhibits the image to overlap figure 2 (a) and (b), and the white lines indicate the spark lines. The maximum brightness intensities at $-0.4 \text{ mm} < y < 0.4 \text{ mm}$ and in steps of 0.08 mm were detected at the various time-dependent x -positions at in each spark image. The arrows in figure 2 (c) indicate the displacements in the x -direction, Δx , within the time interval of the camera, Δt , and the velocities were calculated by Δx divided by Δt . Furthermore, it is qualitatively found that the brightness intensity of the spark line in figure 2 (b) was lower than that in figure 2 (a). This is caused by the diffusion of the ionized air as time advances, and its diffusion induces to hardly detect the maximum brightness intensity in images, which gives the

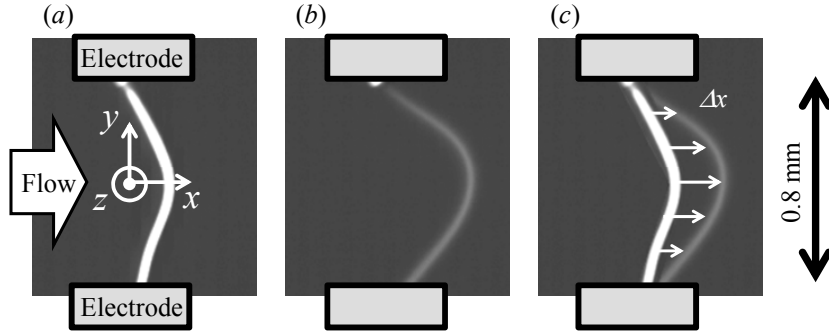


Figure 2: Instantaneous images in single air jet flow through a channel obtained by the spark tracing method at (a) $t = t_0$ and (b) $t = t_0 + \Delta t$. White lines indicate spark lines. (c) The spark line at the image for $t = t_0$ is overlapped with that at $t = t_0 + \Delta t$. The displacement between both spark lines, Δx , is divided by Δt , provides the velocity distribution.

measurement error. For the evaluation of its error, the volumetric flow rates were calculated from the velocity distributions for the case of the second and subsequent voltage applications, except the first application, because the first application was used to make a pathway through spark lines. On the basis of the flow rate at the second application, it was made clear that their rates were decreased by approximately 1% and 2% at the third and fourth applications, respectively. To reduce the measurement error, we obtained the spark line image of the second voltage application and calculated the velocity distributions. In each experiment, 2,000 pair images of spark lines were randomly selected from 5,000 successive images, and the average velocities and their standard deviations were evaluated from 1,000 velocity data. In addition, all the Cartesian coordinate systems of the present study obey the coordinate as shown in figure 2 (a), and the direction of gravitational force is the negative z -direction.

3. EXPERIMENTAL SETUP

3.1 Experimental Apparatus

Figure 3 shows the schematic of the experimental apparatus, and its piping system was developed by using polyurethane tubes. The pressure of air discharged from the bellows pump was controlled by using the regulator and the mass flow controller, and then, the air jet flow was formed through one or two channels. In sections 4.1–4.3, the single air jet flow with a sub-millimeter-scale was set by using one 0.8 mm-square channel (VitroCom, Inc., Square tubing, ST8280, 0.8 mm (width) \times 0.8 mm (height) \times 50 mm (length)) and equipping two needle-typed electrodes at the exit of channel, as shown in figures 3 (a) and (b). In section 4.4, for the investigation of the effect of the gas temperature on the velocity detection, the mixing air jet flow with different temperatures through two channels with an angle of 45 degrees was used as shown in figures 3 (c) and (d). The air flow discharged from the mass flow controller was bifurcated into the air flow of 297 K ($y < 0$) and the other air flow of 318 or 343 K ($y > 0$) heated by using the variable non-flame air heater. For the visualization of the whole flow field, two electrodes (hereinafter referred to as the linearly-aligned electrodes) were located along the x -direction, which enables to discharge sparks intermittently. The gap width between two electrodes was increased towards the downstream in the x -direction, whose arrangement was based on the characteristics of air jet flow.

3.2 High Voltage System with High Frequency

For the acquisition of clear spark line images, it is required to utilize a high voltage system with a high frequency and a short pulse width. The electric transformer of its system was self-produced by utilizing the ignition coil system, which was comprised of the DC power supply, the transistor with the bias circuit using the pulse generator, and the ignition coil. The back electromotive force was generated by the self-induced electromotive force at the primary winding. The pulse duration at the secondary winding was modulated by controlling the pulse duration of the bias circuit, which was set at 5 μ s. This fact gives to make the spark lines with the frequency of up to 2×10^5 Hz, and additionally, it was necessary for the measurement principle that the frequency was more than 1×10^3 Hz as noted in section 2.1. Based upon the displacement of spark lines and the time resolution of measurement system as described in section 3.3, the present study set up the frequency of the high voltage system with 1×10^4 Hz. Furthermore, the present ignition coil system achieved 50 times the transformer ratio, which enables to apply the voltage of a few kV to the electrodes as shown in figure 3.

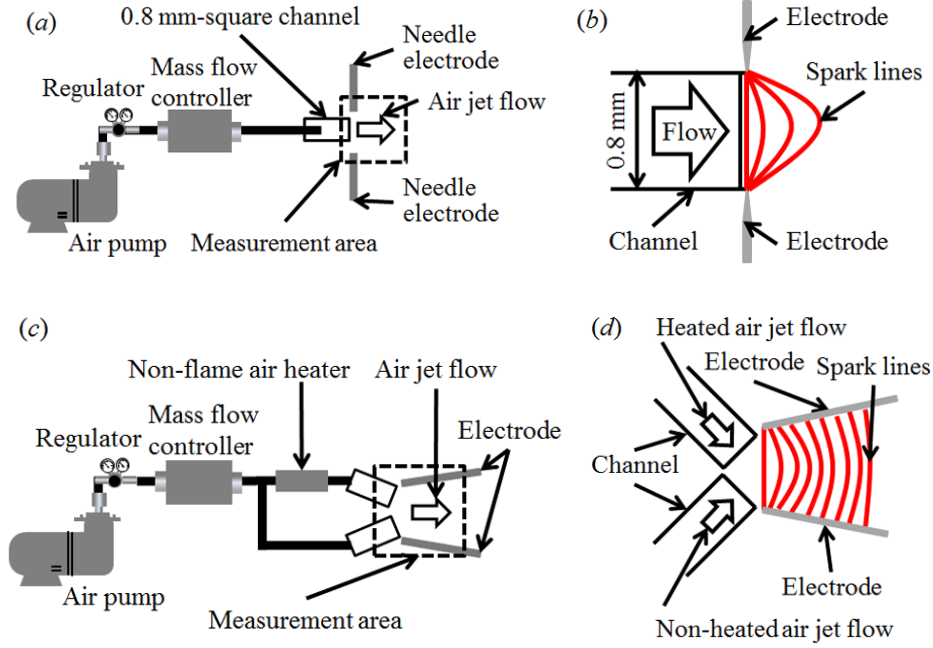


Figure 3: (a) Schematic of experimental apparatus using single air jet flow and (b) detail drawing of measurement area. (c) Schematic of experimental apparatus using mixing air jet flow through two channels and (d) detail drawing of measurement area.

3.3 Optical Measurement System

The optical measurement system was comprised of the high speed CMOS camera (Photron USA, Inc., FASTCAM SA1.1, 12 bits, 756×756 pixels @ 1×10^4 Hz, 1024×1024 pixels @ 125 Hz) and the 10 or 20 \times magnification objective lenses (Nikon Corp., CFI), and its system were equipped at the upper side of channel. In sections 4.1–4.3, the frame rate of camera was set at 1×10^4 Hz for the acquisition of one spark line in each image. In section 4.4, for the visualization of whole measurement area, the rate was at 125 Hz, which can obtain 80 spark lines in each image.

4. RESULTS AND DISCUSSION

4.1 Velocity Measurement of Sub-Millimeter-Scale Gas Flow

The velocity distributions of the single air jet flows as shown in figures 3 (a) and (b) were measured by using the spark tracing method, whose Reynolds numbers (Re) were 65 and 135. Figure 4 shows the obtained velocity distributions, and the solid and dashed lines represent the velocity distributions calculated using the following theoretical equation [27],

$$u = \frac{1}{2\mu} \left(-\frac{dp}{dx} \right) (b^2 - z^2) - \frac{16b^2}{\pi^3 \mu} \left(\frac{dp}{dx} \right) \sum_{n=1}^{\infty} \frac{(-1)^n}{(2n-1)^3} \cos \frac{(2n-1)\pi z}{2b} \frac{\cosh((2n-1)\pi y/2b)}{\cosh((2n-1)\pi a/2b)} \quad (1)$$

where u is the streamwise velocity in the x -direction, μ is the viscosity of the fluid, dp/dx is the pressure gradient, a is the half width of the microchannel in the y -direction, and b is the half depth in the z -direction. As shown in figure 4, the velocities of the experiments were 10–30% smaller than those of the theoretical equation, and this measurement error might be induced by the following two factors.

(a) The brightness intensities obtained from the spark tracing method were integrated in the z -direction. Estimated from the image processing, the diameter of the spark lines in the present study was approximately 0.1 mm, which was one-eighth of the channel depth that is 0.8 mm. This fact might provide the measurement error due to the velocity gradient in the z -direction.

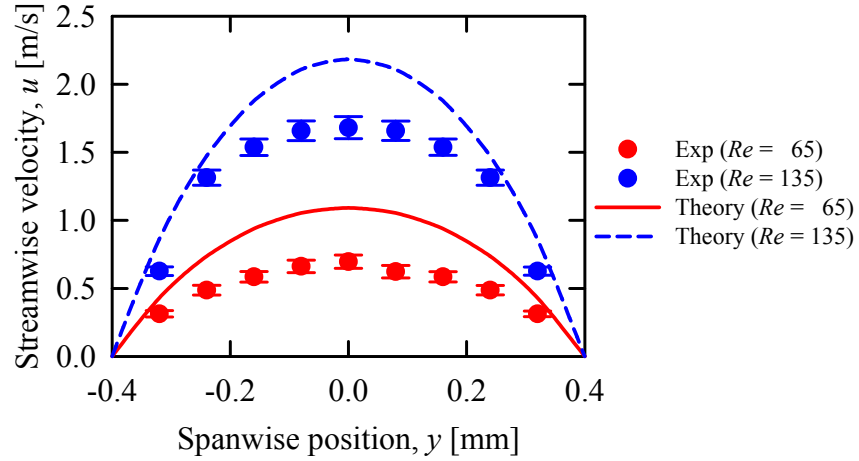


Figure 4: Comparison between the experimental velocity distributions obtained by spark tracing method and the theoretical velocity distributions. The error bars indicate the standard deviations.

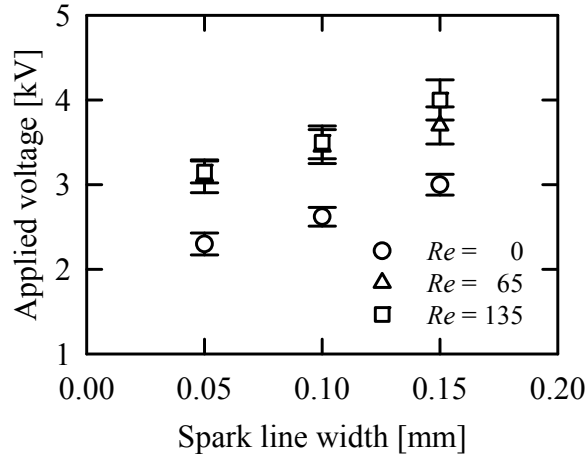


Figure 5: The relationship between applied voltages and spark line widths. The error bars indicate the standard deviations.

(b) For the application to a flow with a large velocity gradient, the spark line passes through a pathway that is smaller than the curvature of the actual velocity distribution due to the short circuit, and it was well known that the obtained velocities are underestimated [28]. This is caused by the diffusion of the ionized air, and the spark line generally goes through a pathway with a minimum electric resistance that is different from a pathway of theoretical equation.

Since the cross-section of the used channel was square-shaped, the theoretical velocity distributions in the x - y plane as shown in figure 4 were equal to those in the x - z plane. The measurement error due to the velocity gradient within $-0.05 \text{ mm} < z < 0.05 \text{ mm}$ was evaluated to be 2–8%, while the experimental data in figure 4 showed 10–30% smaller than the velocities from the theoretical equation. Thus, the above factor (a) is not likely to be considered as the measurement error, and it is required to evaluate the effect of the ion diffusion on the velocity detection as mentioned in the factor (b).

4.2 Velocity Correction Technique for Spark Tracing Method

For the evaluation of the effect of the factor (b) in section 4.1, it is expected to examine the relationship between the spark line widths and the measured velocity distributions. If the measured velocity becomes increased by decreasing the spark line width, we consider that the differences between the velocities from the theoretical equation and the velocities to limit the spark line width to 0 mm become smaller than the differences as shown in figure 4. To verify the above assumption, it is significant to measure velocity distributions under the conditions with several spark line widths. Since the spark line width is varied with a change in the applied voltage, the relationship between the two was experimentally explored as shown in figure 5. It was successful to produce three types of spark line widths of 0.05, 0.10 and 0.15 mm under each flow condition of $Re = 65$ and 135, and this result indicates that the spark line width was increased with an

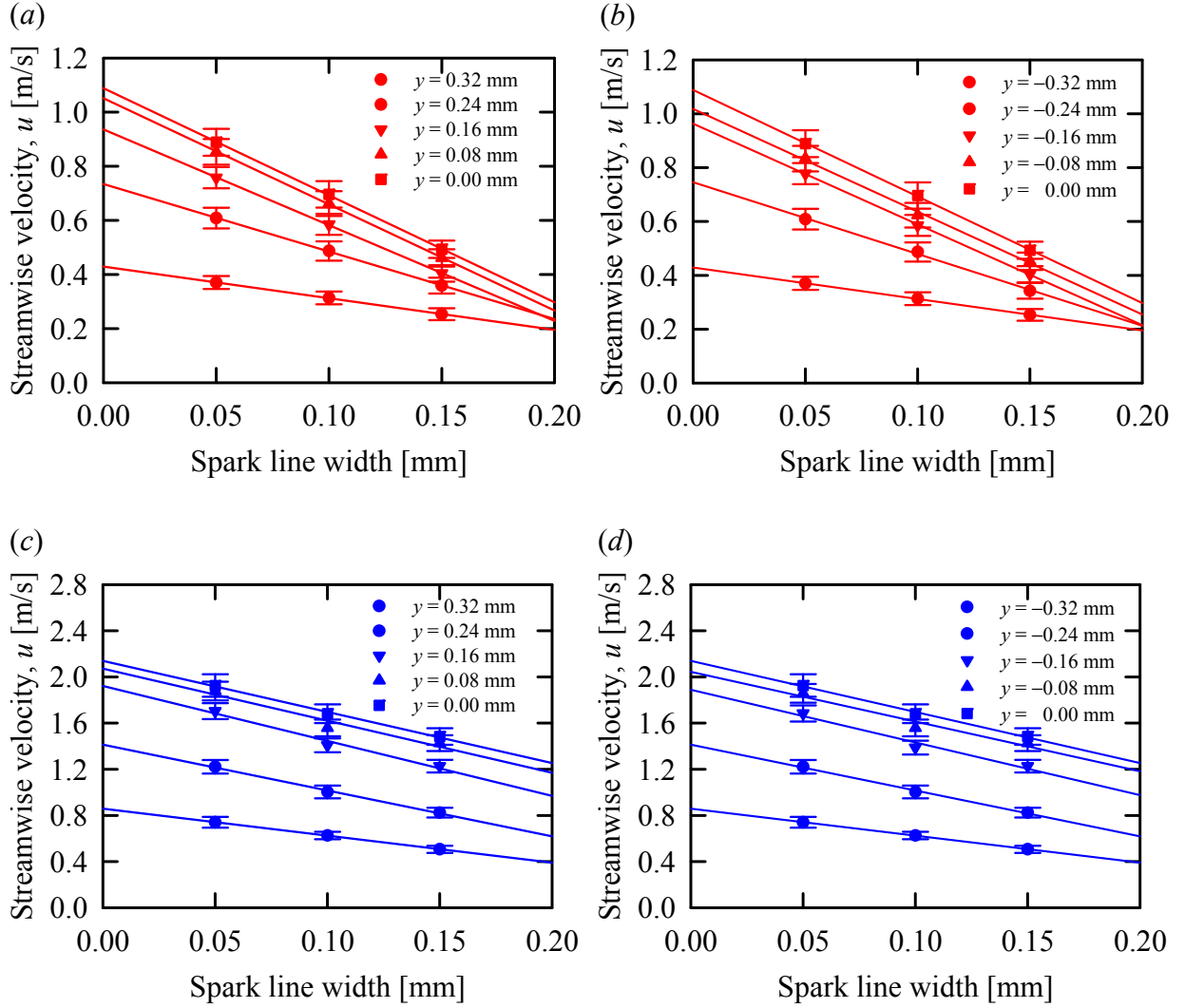


Figure 6: Streamwise velocities obtained by the spark tracing method when using spark line widths of 0.05 mm, 0.10 mm and 0.15 mm at (a) $y > 0$ mm and (b) $y < 0$ mm for $Re = 65$ and (c) $y > 0$ mm and (d) $y < 0$ mm for $Re = 135$. The solid lines were calculated by the least-squares method. The error bars indicate the standard deviations.

increase in the applied voltage. The velocity distributions were measured using each spark line width under the same experimental conditions in figure 4, and the streamwise velocities are represented in figure 6. These data were arranged using the velocities at the same y -position in terms of the spark line widths, and the solid lines exhibit the first-order fitting curves calculated by using the least-squares method. The result indicates that the obtained velocities were increased with a decrease in the spark line widths, and this fact suggests that the pathway through the actual spark line approaches the path estimated from the theoretical velocity distribution. This is caused by decreasing the width of the pathway through which the spark line is possible to pass. The velocities to limit the spark line width to 0 mm were estimated from the fitting curves, which corresponded to the velocities expressed as 0.00 mm in figure 6. Figure 7 indicates the result of a comparison between the velocities when the width was 0.00 mm and those from the theoretical equation [27], and it was found that the estimated data were agreed well with the theoretical data. The present study proposes the new velocity correction technique for the spark tracing method, which is a sequence of the above procedures. Furthermore, the lower limit of the velocity measurement using this method is defined from the frequency of the high voltage system with 1×10^4 Hz and the interval of the spark lines [22]. Its interval is estimated from the pixel displacements of spark lines in the camera images, whose lower limit is approximately 10 pixels on the basis of the spark line width. Considering the pixel size of the camera and the magnification of the objective lens, the lower limit of this method was evaluated to be 0.2 m/s. In addition, the present method with the velocity correction technique was validated by using the numerical simulation as discussed for details in section 4.3.

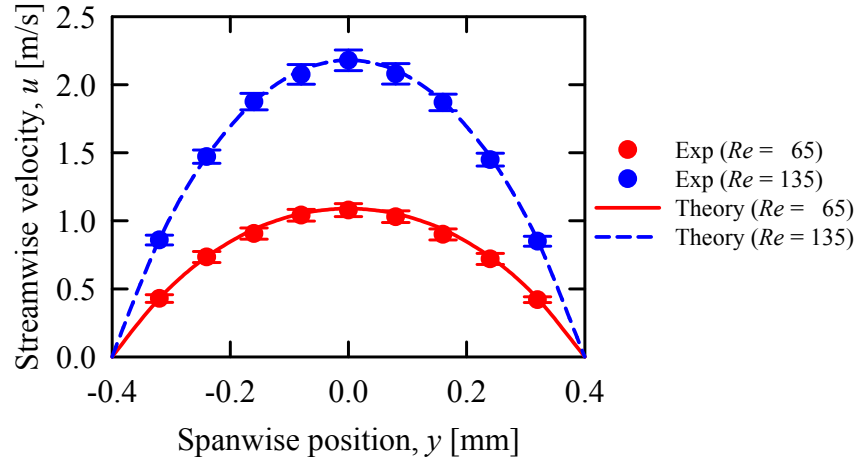


Figure 7: Comparison between the experimental velocity distributions obtained by the spark tracing method with correction and the theoretical velocity distributions. The error bars indicate the standard deviations.

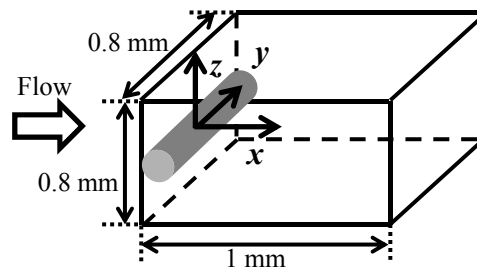


Figure 8: Schematic diagram of the calculation domain by numerical simulation. Gray area shows nitrogen ions as the initial condition.

4.3 Numerical Investigation on Effect of Ion Diffusion on Velocity Detection

In order to validate the proposed correction technique, the effect of the diffusion of the ionized air on the velocity detection was quantitatively investigated by the numerical simulation, which was calculated by using the general-purpose computational fluid dynamics software (CD-adapco, STAR-CCM+). The discretization method used in its software employs the finite volume method, and the calculating area of $0.8 \text{ mm} \times 0.8 \text{ mm} \times 1.0 \text{ mm}$ as shown in figure 8 was divided into 3,251,715 parts by using the polyhedral mesh with the averaged 10-15 dimensions. To simulate the same conditions as the experiments in section 4.2, the unsteady flow field was calculated by using the numerical results of the steady-state flow as the initial condition. Each circular cylinder with the diameter of 0.05, 0.10 and 0.15 mm was set as the ion layer through the spark lines at $x = 0 \text{ mm}$ and $z = 0 \text{ mm}$, which corresponds to the gray area in figure 8. Its layer with the physical property of nitrogen ion was given as the initial condition during $5 \mu\text{s}$, whose diffusion coefficient was $3.0 \times 10^{-5} \text{ m}^2/\text{s}$. The present study calculated the time evolution of nitrogen ion concentration distributions by setting the time step of $1.0 \times 10^{-6} \text{ s}$, and the typical result is illustrated in figure 9. This result indicates the time evolution of ion concentration distributions in x - y planes at $t = t_0$ and $t = t_0 + 100 \mu\text{s}$ under all the initial conditions of ion layer, and these data were normalized using the initial ion concentration. It was observed that the nitrogen ion was extensively diffused as time advances due to the advection and the ion concentration gradient. From the viewpoint of the quantitative evaluation, when the spark line width was assumed to be more than 40% of the initial ion concentration, it was made clear that the width of diffused ion was approximately twice the width of the initial condition.

For the investigation of the relationship between the ion distribution and the pathway of spark line, the electric resistance of each pathway was evaluated because an actual spark line goes through a pathway with a minimum electric resistance as described in section 4.1. The electric resistance in an air flow, R , is expressed as the following equation using the path length, L , and the cross-section of spark, S ,

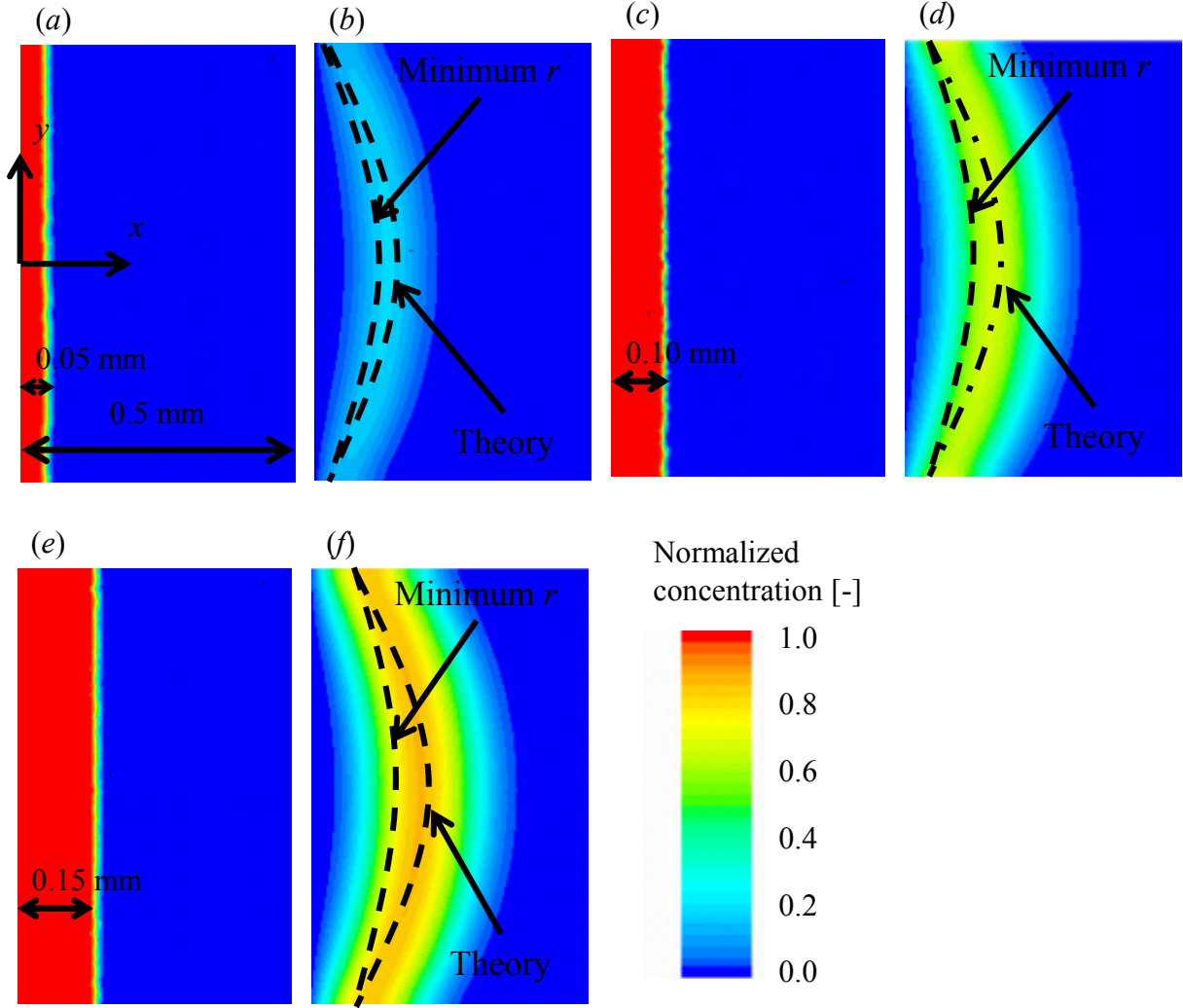


Figure 9: Time evolution of nitrogen ion concentration distributions obtained by numerical simulation at (a) $t = t_0$ and (b) $t = t_0 + 100 \mu s$ using ion layer with the diameter of 0.05 mm, (c) $t = t_0$ and (d) $t = t_0 + 100 \mu s$ using ion layer with the diameter of 0.10 mm, and (e) $t = t_0$ and (f) $t = t_0 + 100 \mu s$ using ion layer with the diameter of 0.15 mm.

$$R = \frac{L}{\sigma \cdot S} = \frac{L}{e^2 \mu_j \cdot n_i \cdot S} \quad (2)$$

where σ is the electrical conductivity, e is the elementary charge, μ_j is the electron mobility, and n_i is the density of ion. It was obvious from equation (2) that the electric resistance is proportional to the path length and inversely proportional to the density of ion. The present study proposes the new parameter to estimate the electric resistance, r , using L and n_i (hereinafter referred to as the resistance parameter), which was given by the following equation,

$$r = \oint \frac{1}{n} dL \quad (3)$$

The resistance parameters were evaluated with respect to 30 pathways including the paths from the theoretical equation and the experimental results without the correction. In figure 9 (b), the dashed-dotted line indicates the pathway from the theoretical equation, and the pathway with the minimum resistance parameter is represented as the dashed line. Since the spark line passes the pathway with the minimum electric resistance, it was qualitatively observed that the velocity distribution from the experiment was smaller than that from the theoretical equation. Figure 10 exhibits the relationship between the electric resistances and the path lengths of the spark lines. The resistance parameters of the vertical axis were normalized using the resistance parameters under the experimental conditions without the correction, r_{exp} , which means that the data of $r/r_{exp} = 1$ correspond to the experimental results. On the other hand, the path lengths of

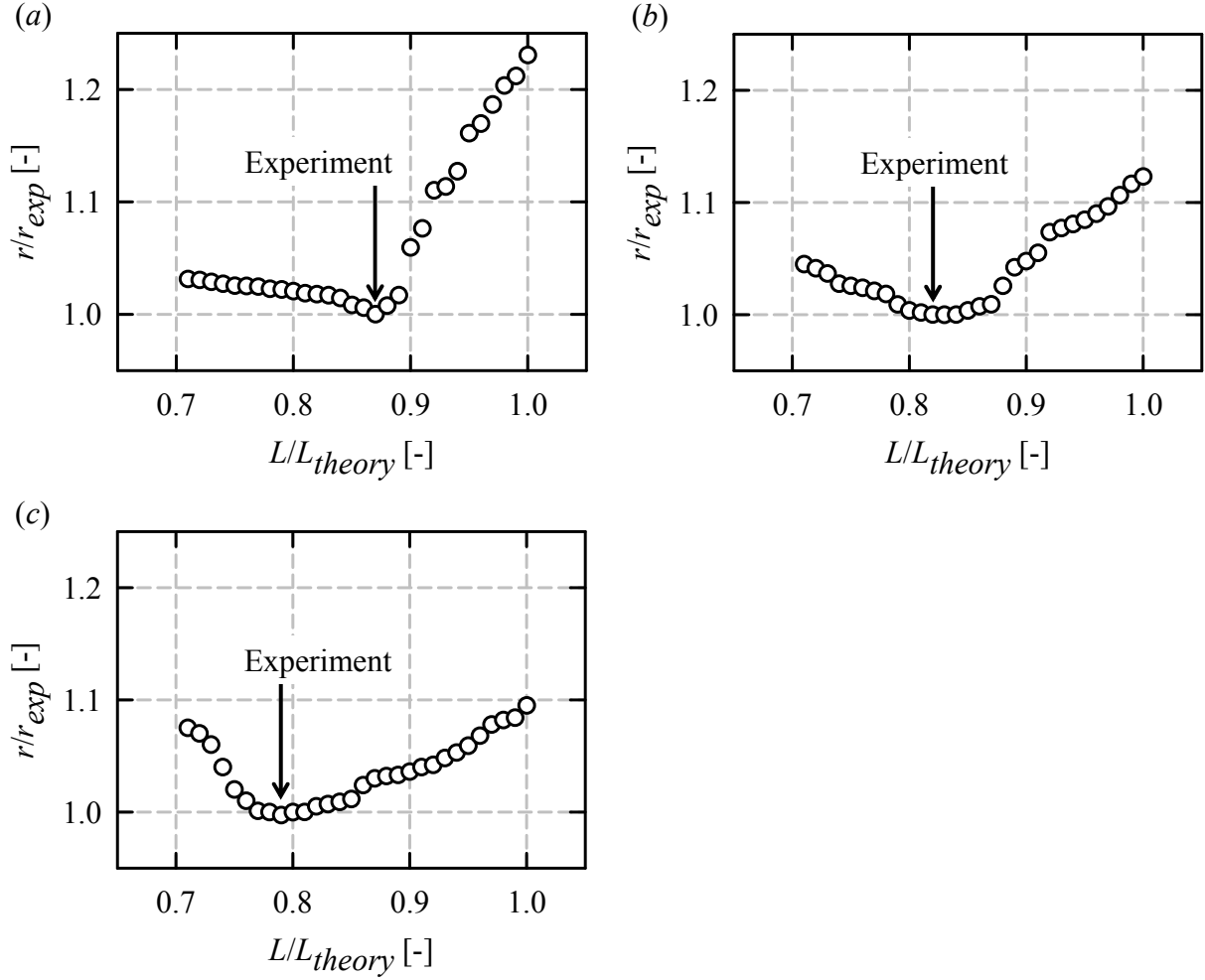


Figure 10: Relationships between the electric resistances and path lengths of spark line which were obtained by numerical simulation under conditions of spark line widths of (a) 0.05 mm, (b) 0.10 mm and (c) 0.15 mm.

the horizontal axis were normalized using the path lengths estimated from the theoretical equation, L_{theory} , and hence the theoretical results are represented as the data of $L/L_{theory} = 1$. These results indicate that the resistance parameters under the conditions of all the pathways were qualified as $r/r_{exp} \geq 1$ and the minimum resistance parameters were shown under the experimental conditions. Therefore, it was made clear that the measurement error of the spark tracing method under the present experimental conditions was caused by the factor (b) as described in section 4.1.

Furthermore, for further insight into the relationship between the velocity distribution and the pathway of spark line, the velocity distributions of the pathways with the minimum r/r_{exp} were calculated under the conditions of each spark line width by using the numerical simulation, and their pathways were equal to the experimental results. Figure 11 shows the streamwise velocities divided by the theoretical velocities, u/u_{theory} , and these data were ordered by using the same procedure as figure 6. For the velocities at the same y -position in terms of the spark line widths, the first-order fitting curves were calculated by using the least-squares method, which were expressed as the dashed lines. This result reveals that all the u/u_{theory} were nearly equal to 1 when the spark line width was 0 mm, which means that the experimental results with the correction are agreed well with the theoretical results. Thus, these above facts give the availability and validity of the velocity correction technique proposed in section 4.2.

4.4 Experimental Investigation on Effect of Temperature Change on Velocity Detection

In order to examine the effect of the temperature change on the velocity detection, the spark tracing method with the correction technique was applied to the mixing air jet flows, whose experimental apparatus are shown in figures 3 (c) and (d). In this experiment, the linearly-aligned electrodes were employed, because the active electrode area was increased towards the streamwise direction, which enables us to visualize the spark lines extensively in comparison with the needle-typed electrodes used in sections 4.1–4.3. The previous study [28] has reported that the use of the linearly-

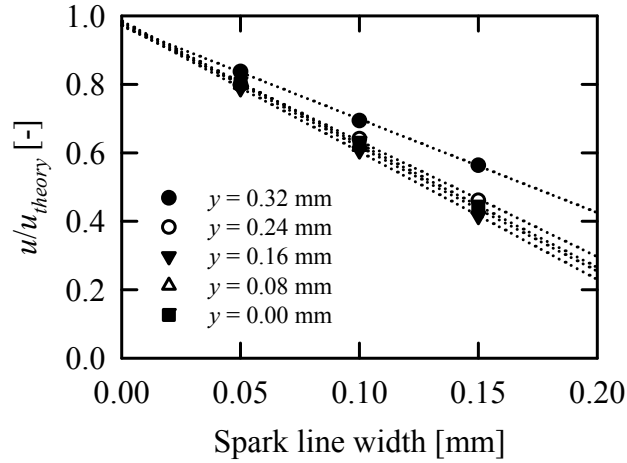


Figure 11: Streamwise velocities obtained by numerical simulation under conditions of spark line widths of 0.05 mm, 0.10 mm and 0.15 mm. Dashed lines were calculated by the least-squares method.

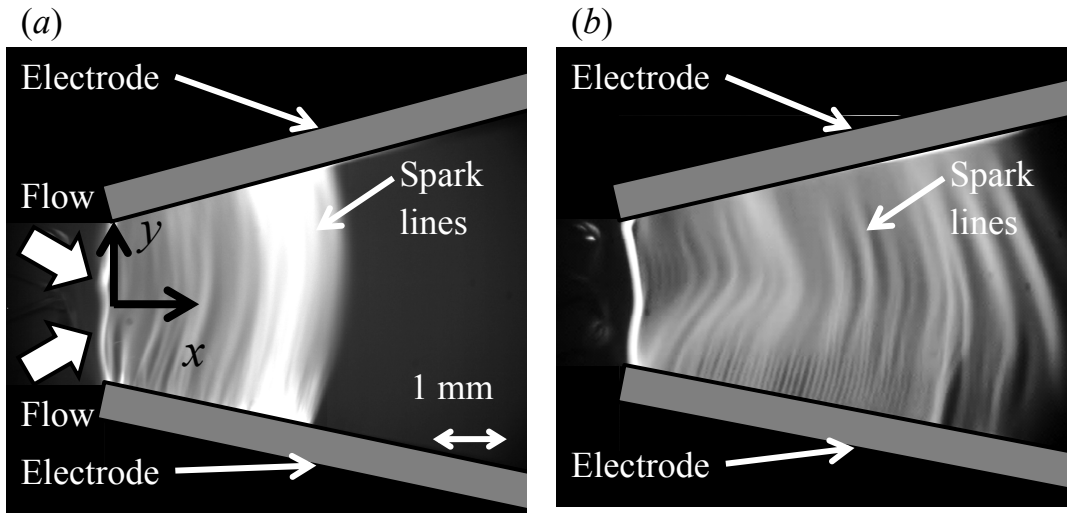


Figure 12: Instantaneous images in mixing air jet flow through two channels at $Re = (a)$ 65 and (b) 135 obtained by the spark tracing method. White lines indicate spark lines.

aligned electrodes induces the error on the order of 1% for the velocity measurement, because the spark line width are increased by the order of 10%. On the other hand, since the present study proposed the velocity correction technique using the relationship between the spark line widths and the velocity distributions, the effect of the difference in the electrode arrangements on the velocity detection is considered to be negligible. Figure 12 illustrates the instantaneous images of the mixing air jet flows through two channels in which both flows have the same temperature of 297 K, and their Reynolds numbers were (a) 65 and (b) 135. It was observed that the existing area of spark lines at $Re = 135$ was larger than that at $Re = 65$, because the interval of spark lines was increased with an increase in the flow velocity. Figure 13 plots the streamwise velocity distributions at $x = 1, 2, 4$ and 6 mm, whose experiments were conducted under the same conditions as figure 12, and their data were obtained by using the correction technique. The distances between two electrodes in the y -direction were estimated to be 3.0, 3.4, 4.2 and 5.0 mm at each x -position by using the image processing. It was observed that the velocity distributions at $x = 1$ and 2 mm have the maximum values at $y = 0$ mm and the nearly uniform distributions were shown towards the downstream, e.g., the distribution at $x = 6$ mm. At the center position in the y -direction, the velocities at $x = 6$ mm were approximately 50% smaller than those at $x = 1$ mm under both conditions with $Re = 65$ and 135 , which was qualitatively agreed with the velocity distribution of the two-jet flow with the low Reynolds number.

Figure 14 shows the streamwise velocity distributions in the mixing air jet flows whose temperatures were set to be 318 and 343 K at $y > 0$ mm and 297 K at $y < 0$ mm. This setup corresponds to the temperature differences of $\Delta T = 20$ and 45 K, respectively. The velocity data of $\Delta T = 0$ K as shown in figure 13 were also added to figure 14, and it was

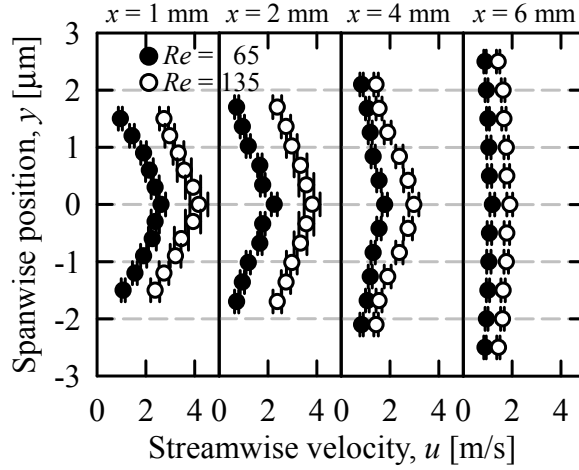


Figure 13: Streamwise velocity distributions in the mixing air jet flow through two channels obtained by the spark tracing method with correction. The error bars indicate the standard deviations.

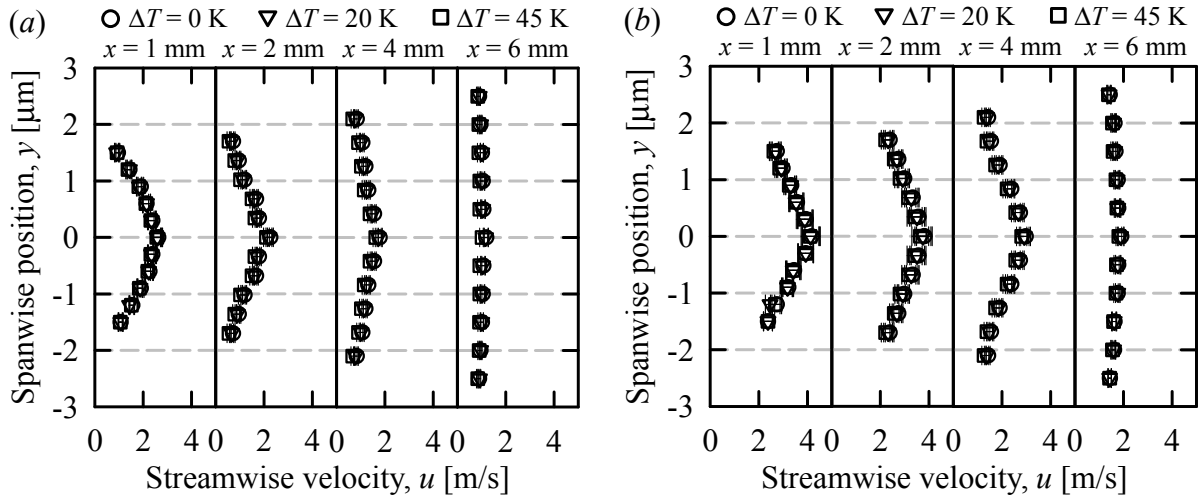


Figure 14: Streamwise velocity distributions in mixing air jet flow through two channels at $Re = (a)$ 65 and (b) 135 obtained by the spark tracing method with correction. The air flow temperatures were set to be 318 and 343 K at $y > 0$ and 298 K at $y < 0$. The error bars indicate the standard deviations.

made clear that the temperature change does not influence the velocity detection. Grashof numbers under the conditions of $\Delta T = 20$ and 45 K were estimated to be 1.5 and 3.1, respectively, whose characteristic length was the channel width of 0.8 mm. Even if there are the temperature changes in gas flow fields, the spark tracing method with the present correction technique has the advantage to measure the velocity distributions in sub-millimeter-scale gas flows without another calibration, within the small buoyancy conditions.

5. CONCLUSIONS

The spark tracing method was applied to the velocity measurements of gas flows with a sub-millimeter-scale. In order to obtain the clear spark line images, the high voltage system of a few kV with the high frequency of 1×10^4 Hz was self-produced, and the measurement system was developed by using the high-speed CMOS camera equipped with the objective lens, whose time resolution was 0.1 ms. The air jet flows with a sub-millimeter-scale were formed through one or two 0.8 mm-square channels, and their streamwise velocities were measured at the exit of channel. The important conclusions obtained from this study are summarized below.

The velocities obtained by using the spark tracing method were 10–30% smaller than those estimated from the theoretical equation. To reduce this measurement error, the novel velocity correction technique was proposed, which

was based upon the relationship between the spark line widths and the measured velocities. The corrected velocities were agreed well with the theoretical results.

For the validation of the proposed correction technique, the time evolution of ion concentration distributions was calculated by using the numerical simulation, which was considered with the ion diffusion phenomena. The electric resistances were estimated from the ion concentration distributions, and it was obvious that the spark lines obtained from the experiments passes through the pathways with the minimum electric resistance. The velocity distribution of the pathways with the minimum resistance was calculated by using the numerical simulation. These data were processed by using the proposed correction technique, which were identical to the theoretical results.

The effect of the temperature change on the velocity detection was evaluated using the spark tracing method with the correction technique. Under the conditions of gas flows with different temperatures of the order of 10 K, it was confirmed that the temperature change hardly affects the velocity detection and the present technique enables us to measure the velocity distributions in sub-millimeter-scale gas flows.

ACKNOWLEDGEMENTS

This work was subsidized by Grant-in-Aid for Scientific Research (S) (No. 21226006) from the Japan Society for the Promotion of Science.

REFERENCES

- [1] Reyes, D. R., Iossifidis, D., Auroux, P. A. and Manz, A., "Micro total analysis system. 1. Introduction, theory and technology", *Analytical Chemistry*, Vol. 74, (2002), pp. 2623–2636.
- [2] Auroux, P. A., Iossifidis, D., Reyes, D. R. and Manz, A., "Micro total analysis system. 2. Analytical standard operations and applications", *Analytical Chemistry*, Vol. 74, (2002), pp. 2637–2652.
- [3] Günther, A. and Jensen, K. F., "Multiphase microfluidics: from flow characteristics to chemical and materials synthesis", *Lab on a Chip*, Vol. 6, (2006), pp. 1487–1503.
- [4] Sinton, D., "Microscale flow visualization", *Microfluidics and Nanofluidics*, Vol. 1, (2004), pp. 2–21.
- [5] Santiago, J. G., Wereley, S. T., Meinhart, C. D., Beebe, D. J. and Adrian, R. J., "A particle image velocimetry system for microfluidics", *Experiments in Fluids*, Vol. 25, (1998), pp. 316–319.
- [6] Lindken, R., Rossi, M., Große, S. and Westerweel, J., "Micro-particle image velocimetry (μ PIV): Recent developments, applications, and guidelines", *Lab on a Chip*, Vol. 9, (2009), pp. 2551–2567.
- [7] Wereley, S. T. and Meinhart, C. D., "Recent advances in micro-particle image velocimetry", *Annual Review of Fluid Mechanics*, Vol. 42, (2010), pp. 557–576.
- [8] Sadr, R., Yoda, M., Zheng, Z. and Conlisk, A. T., "An experimental study of electro-osmotic flow in rectangular microchannels", *Journal of Fluid Mechanics*, Vol. 506, (2004), pp. 357–367.
- [9] Kihm, K. D., Banerjee, A., Choi, C. K. and Takagi, T., "Near-wall hindered Brownian diffusion of nanoparticles examined by three-dimensional ratiometric total internal reflection fluorescence microscopy (3-D R-TIRFM)", *Experiments in Fluids*, Vol. 37, (2004), pp. 811–824.
- [10] Pouya, S., Koochesfahani, M., Snee, P., Bawendi, M. and Nocera, D., "Single quantum dot (QD) imaging of fluid flow near surfaces", *Experiments in Fluids*, Vol. 39, (2005), pp. 784–786.
- [11] Freudenthal, P. E., Pommer, M., Meinhart, C. D. and Piorek, B. D., "Quantum nanospheres for sub-micron particle image velocimetry", *Experiments in Fluids*, Vol. 43, (2007), pp. 525–533.
- [12] Kim, J. K., Kawahashi, M., Hirahara, H. and Iwasaki, Y., "Experimental analysis of oscillatory airflow in a bronchiole model with stenosis", *Journal of Visualization*, Vol. 12, (2009), pp. 109–118.

- [13] Gendrich, C. P. and Koochesfahani, M. M., “A spatial correlation technique for estimating velocity fields using molecular tagging velocimetry (MTV)”, *Experiments in Fluids*, Vol. 22, (1996), pp. 67–77.
- [14] Koochesfahani, M. M., Cohn, R. and MacKinnon, C., “Simultaneous whole-field measurements of velocity and concentration fields using a combination of MTV and LIF”, *Measurement Science and Technology*, Vol. 11, (2000), pp. 1289–1300.
- [15] Paul, P. H., Garguilo, M. G. and Rakestraw, D. J., “Imaging of pressure- and electrokinetically driven flows through open capillaries”, *Analytical Chemistry*, Vol. 70, (1998), pp. 2459–2467.
- [16] Ross, D., Johnson, T. G. and Locascio, L. E., “Imaging of electroosmotic flow in plastic microchannels”, *Analytical Chemistry*, Vol. 73, (2001), pp. 2509–2515.
- [17] Sinton, D. and Li, D., “Microfluidic velocimetry with near-wall resolution”, *International Journal of Thermal Sciences*, Vol. 42, (2003), pp. 847–855.
- [18] Senga, Y., Nakamura, T., Fukumura, H., Ichiyanagi, M. and Sato, Y., “Near-wall motion of caged fluorescent dye in microchannel flows obtained from evanescent wave molecular tagging”, *Journal of Fluid Science and Technology*, Vol. 5, No. 2, (2010), pp. 192–206.
- [19] Andrea, G., Srinivasan, R., Rodney, D., Bowersox, W. and Simon, W., “Two-component molecular tagging velocimetry utilizing NO fluorescence lifetime and NO₂ photodissociation techniques in an underexpanded jet flowfield”, *Applied Optics*, Vol. 48, (2009), pp. 4414–4423.
- [20] Hecht, C., van der Schoot, N., Kronemayer, H., Wlokas, I., Lindken, R. and Schulz, C., “Visualization of the gas flow in fuel cell bipolar plates using molecular flow seeding and micro-particle image velocimetry”, *Experiments in Fluids*, Vol. 52, (2012), pp. 743–748.
- [21] Nakayama, Y. and Aoki, K., “Progress of visualization”, *Journal of Visualization*, Vol. 4, No. 1, (2001), pp. 9–18.
- [22] Kashikajohogakunyumon henshuiuinkai, “Introduction to visualization”, (1994), pp. 50–54, Tokyo Denki University Press, (in Japanese).
- [23] Bernotat, S. and Umhauer, H., “Application of spark tracing method to flow measurements in an air classifier”, *Optical and Quantum Electronics*, Vol. 5, No. 1, (1973), pp. 107–118.
- [24] Nakayama, Y., Yamamoto, T., Aoki, K. and Ohta, H., “Measurement of relative velocity distribution in centrifugal blower impeller”, *Transactions of the Japan Society of Mechanical Engineering Series B*, Vol. 51, No. 461, (1985), pp. 325–332.
- [25] Kawaguchi, K. and Matsui, K., “Flow visualization around the wing of an axial flow fan”, *Transactions of the Japan Society of Mechanical Engineering Series B*, Vol. 51, No. 466, (1985), pp. 1789–1797.
- [26] Matsuo, K., Setoguchi, T. and Yamamoto, Y., “The error in measuring an accelerated flow velocity by a spark tracer method”, *Transactions of the Japan Society of Mechanical Engineering Series B*, Vol. 46, No. 411, (1980), pp. 2150–2158.
- [27] Nagamoto, H., Kobayashi, Y., Otomo, J. and Oshima, E., “Laminar flow characteristics in a rectangular microchannel”, *Kagaku Kogaku Ronbunshu*, Vol. 32, (2006), pp. 293–296.
- [28] Asanuma, T., “Flow visualization handbook”, (1977), pp. 289–293, Asakura Publishing Co., Ltd., (in Japanese)